PART 2

ACTIVE REGIONS

https://doi.org/10.1017/S0074180900071539 Published online by Cambridge University Press

X-RAY SPECTRA OF SOLAR ACTIVE REGIONS

JOHN H. PARKINSON

Mullard Space Science Laboratory, Dept. of Physics and Astronomy, University College London, Holmbury St. Mary, Dorking, Surrey, England

Abstract. The last few years have seen great progress in our understanding of X-ray spectra of solar active regions. This paper demonstrates both the usefulness and the limitations of the techniques, both scientific and instrumental, that have recently become available. Improvements in spectral resolution led to the discovery of weak satellite lines to helium-like ions; the quantitative theory for these lines is also discussed. The observed intensities of the Fe XVII lines are also investigated and found to be in agreement with calculations that allow for cascading processes.

I. Introduction

For many years now it has been recognised that the solar corona has a temperature in excess of one million degrees and emits most of its energy in the X-ray region. However it is only in the last ten years or so that it has been possible to obtain X-ray spectra of sufficient resolution that the dominance of line emission was recognised. Further, it is only in the last three years that spatially resolved high resolution spectra have been obtained. The excellent review by Walker (1972) covers much of this work. Although this Symposium takes place at a time when the Sun is in the 'quiet' part of its cycle, the last few years, as we will see, have been anything but 'quiet' for those working in the X-ray spectral region!

The corona is an object of great interest for the solar astronomer and the atomic physicist alike. By observing the spectrum below approximately 25 Å the solar astronomer can obtain information on the physical state of the plasma with temperatures $\gtrsim 10^6$ K, he can also directly observe the coronal condensations above active regions as they rotate across the solar disc. The atomic physicist is able to observe a plasma which has physical conditions very different to those he is able to create in the laboratory. The spectrum contains lines due to a wide variety of transitions; in addition to the normal allowed electric dipole transitions both magnetic dipole and quadrupole transitions are observed, mainly from H-, He- and Ne- like ions.

This paper does not aim to be a comprehensive review but rather to highlight the techniques, both scientific and instrumental, that are available and to demonstrate both their usefulness and limitations. In a following paper Dr Walker (1975) will discuss more of the implications of some of the observations discussed here. We start by discussing the experimental techniques and some of the improvements that have been made recently in increasing spectral resolution. We will see how this increased resolution has allowed us to use new methods for the diagnosis of the temperature and density structure of coronal features. Finally we investigate the atomic physics that can be derived from X-ray spectral observations. The spectrum emitted by an active region between 2 and 5×10^6 K is very different to that emitted by a flare. We will always restrict ourselves to observations of non-flaring active regions.

Sharad R. Kane (ed.), Solar Gamma-, X-, and EUV Radiation, 45–64.

II. Experimental Techniques

The main dispersive instrument that has been used below 25 Å is the scanning Bragg crystal spectrometer, the diffracted photons being detected by proportional counters. A wide variety of crystals is available with various lattice spacings and rocking curves, so that the choice of crystal can be optimised for the particular problem being studied. Much ingenuity has been shown in building smooth, linear drive systems for scanning the crystals and detectors, and many Bragg angle readout systems have been flown in rocket and satellite experiments.

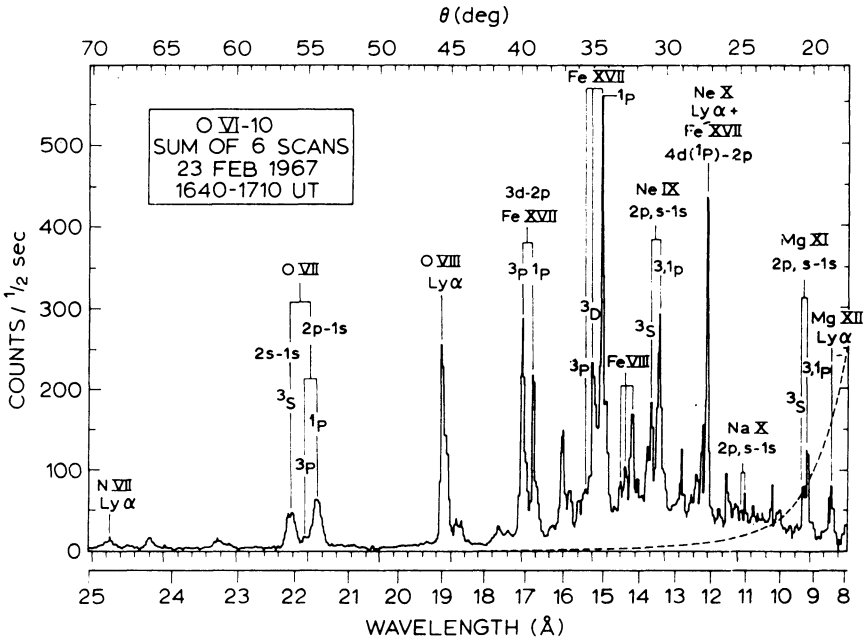

Fig. 1. Non-flare spectrum obtained with a KAP spectrometer on the OVI-10 satellite on 1967, February 23 when the solar X-ray emission was dominated by a single active region (Rugge and Walker, 1968).

The early observations of Blake *et al.* (1965), Fritz *et al.* (1967), Evans and Pounds (1968), Rugge and Walker (1968) and Neupert (1971) were from rocket and satellite instruments which viewed the whole Sun and integrated the emission from the corona and all of the active regions present. Examples of these observations are shown in Figures 1 and 2 and it can be clearly seen that the spectrum is dominated by lines of Fe XVII together with lines from H- and He- like Mg, Ne and O. The spectral resolution is quite low and many lines are blended together.

Figure 3a shows a scan through the Mg XI lines around 9 Å made with a rocket spectrometer that had better spectral resolution than previous instruments. At the time of the rocket flight there were five active regions on the Sun and each one pre-

https://doi.org/10.1017/S0074180900071539 Published online by Cambridge University Press

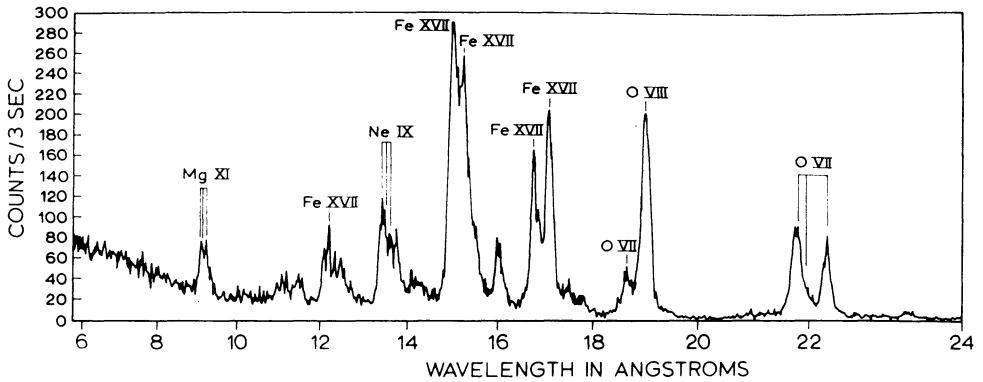

Fig. 2. Non-flare spectrum obtained on 1969, January 27 with a KAP spectrometer on the OSO 5 satellite (Neupert, 1971).

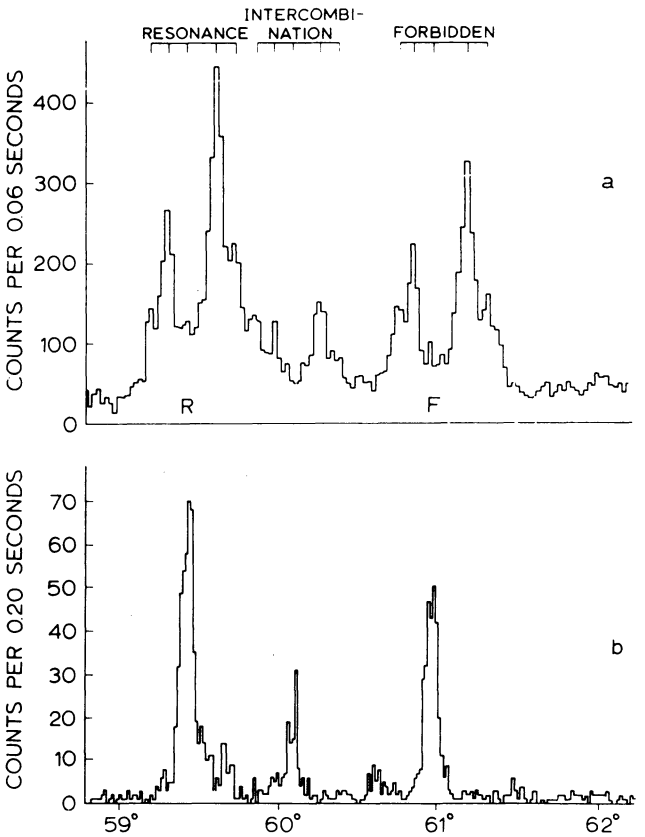

Fig. 3. Scans through Mg XI (a) with an uncollimated spectrometer showing spectra for five active regions (Batstone, 1970). (b) with a spectrometer collimated to 4′ FWHM, showing several satellite lines (Parkinson, 1971a).

https://doi.org/10.1017/S0074180900071539 Published online by Cambridge University Press

sented a slightly different angle of incidence to the crystal. This led to there being five different spectra, each slightly shifted relative to the next. Batstone (1970) was able to deconvolve this data to give the individual spectrum for each active region, by identifying five resonance lines, five intercombination lines and five forbidden lines.

The problem of overlapping spectra has been approached in two ways.

(a) INSTRUMENTS VIEWING A SINGLE REGION

The easiest way to improve the spectral clarity of a set of observations is to remove the contributions from other active regions by restricting the field of view to a single active region. Thus if several active regions are to be observed then they must be observed sequentially.

Figure 3b shows the results obtained by using a spectrometer of the same design as that used to obtain the results in Figure 3a, but with the field of view restricted to 4′ in order to isolate a single active region (Parkinson, 1971a). Here we can see the main lines resolved, there are no overlapping spectra, and many weak satellite lines are observed; these will be discussed in Section IV.

The most useful design of collimator is one where grids are aligned and spaced in a geometrical progression which depends on the hole: bar ratio of the grids. This type of construction has an advantage over the Soller type of collimator as reflections off the slats at grazing incidence are removed. The technique is described in more detail by Parkinson (1971b).

(b) INSTRUMENTS CAPABLE OF PRODUCING SPECTROHELIOGRAMS

Several workers have used devices which scan the whole Sun and remove the need to conduct observations sequentially. Acton *et al.* (1972) collimated their instrument in only one direction, to 1.7′, and scanned this slowly across the solar disc while two spectrometers scanned rapidly through pre-selected parts of the spectrum. The rocket was rolled through approximately 60° and the collimator scanned back across the solar disc. Both of the spectrometers used KAP crystals, one was set to scan through the lines of O VII between 21.38 and 22.27 Å and the other scanned through the lines of Ne IX between 13.34 and 13.78 Å. The crystals scanned their pre-selected wavelength ranges every 1 s and the rocket moved through 1.5′. in 5 s In this way it was possible to derive spectra for each active region present on the solar disc. Figure 4 shows such spectra for a single active region and also the sum of all the spectra from the active regions. The form of the spectra and other information from this rocket flight will be discussed in more detail in Section IV.

A similar method was used by Bonnelle *et al.* (1973) who also used two spectrometers which were collimated in one direction to 3′. This experiment was pointed at the centre of the Sun and rolled about this axis while the spectrometers scanned their pre-set wavelength ranges. Two ADP crystals were used, one covering the range 8.39 to 8.53 Å which contains the Mg XII Lα line, the other the Mg XI lines in the range 9.15 to 9.34 Å. A wavelength scan took 17.3 s and the payload rolled at a rate of $20.2^{\circ}\ s^{-1}$. ADP has a narrow rocking curve so this was exploited to give both spectral

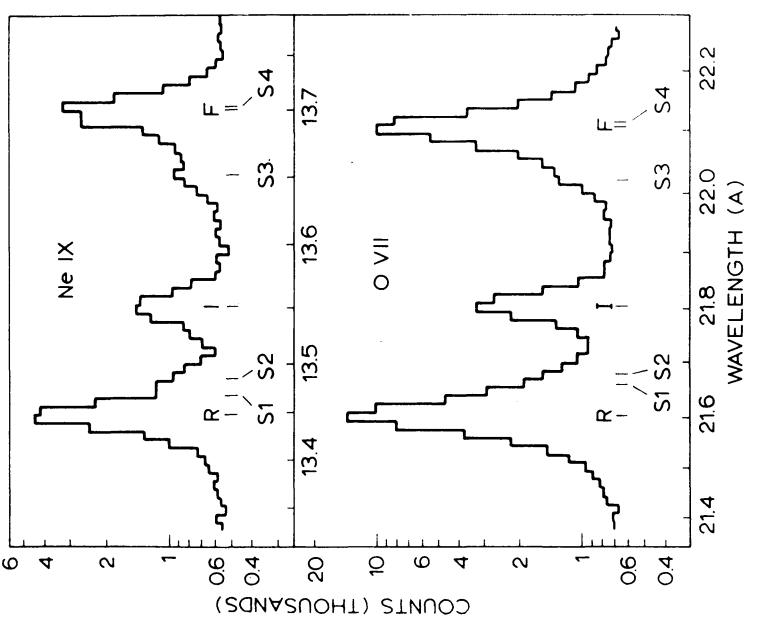

Fig. 4a.

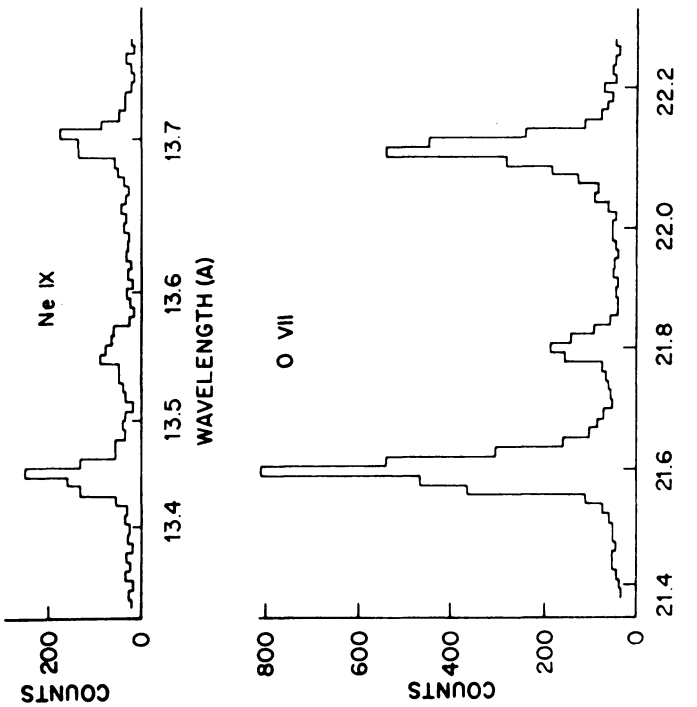

Fig. 4b.

Fig. 4a–b. Scan through Ne IX and O VII. (Acton *et al.*, 1972). (a) for the whole Sun. (b) for a single active region.

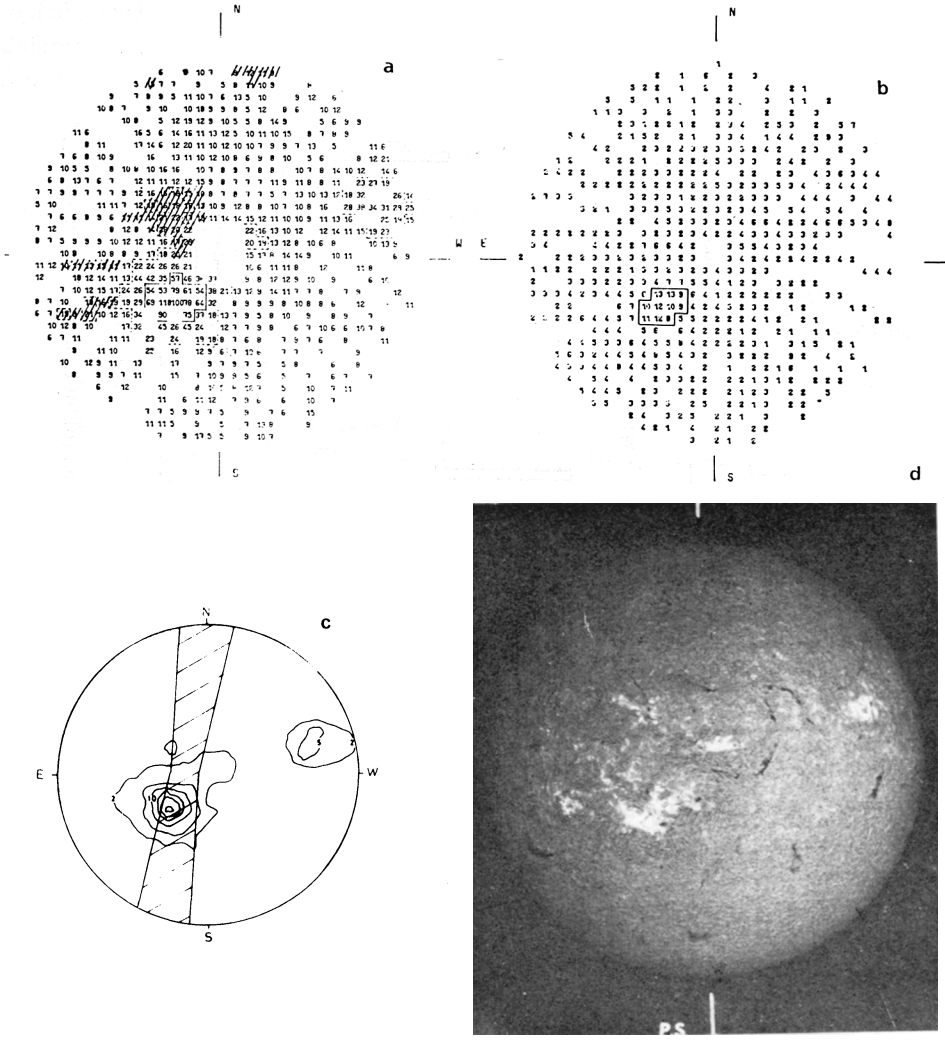

Fig. 5. Comparison by Bonnelle *et al.* (1973) of (a) Spectroheliogram in the resonance line of Mg XI. (b) Spectroheliogram in the Lα line of Mg XII. (c) 8.4–9.6 Å map from OSO 5. (d) Hα spectroheliogram.

and spatial resolution, and spectroheliograms were constructed in a single line with a resolution of about 1′. Figure 5 shows two such spectroheliograms, one is in the resonance line of Mg XI the other in the Lα line of Mg XII, these are compared with an Hα image and an OSO-5 8.4–9.6 Å map, (this wavelength range is dominated by lines of Mg XI and XII, Parkinson and Pounds (1971)) and there is good agreement between these two quite different instruments.

A very different technique for obtaining spectra from several active regions simultaneously has been proposed by Brabban *et al.* (1971). This involves placing a rotation modulation collimator in front of a crystal spectrometer and reconstructing an

https://doi.org/10.1017/S0074180900071539 Published online by Cambridge University Press

image of the Sun in the radiation emitted in each spectral line. The first results (Brabban, 1973) showed that this technique was successful when used in a rocket experiment.

III. The Analysis of an Active Region X-Ray Spectrum

In order to make use of the intensity of a line it must be expressed in energy units by taking into account the instrumental parameters.

The line flux is given by

$$E = \frac{2 \times 10^{-8} N\omega}{AR_c \lambda P T_1 T_2} \text{ erg cm}^{-2} \text{ s}^{-1}, \tag{1}$$

where N is the number of counts in the line; ω is the crystal scan rate in radians s^{-1}; A is the effective crystal area; R_c is the crystal integrated reflection coefficient in radians; λ is the wavelength of the line; P is the photon detection efficiency at wavelength λ; T_1 is the atmospheric transmission at wavelength λ; and T_2 is the transmission of the collimator.

Some of these parameters are comparitively easy to measure or calculate, others are more difficult. For example the reflectivity of the crystals is an important parameter and Leigh and Evans at the University of Leicester and Blake at the University of Chicago have spent many hours carefully measuring the variation of this parameter with wavelength for many crystals.

In order to analyse the spectrum of an active region the lines must first be identified correctly, in general this requires both good spectral resolution and accurate theoretical predictions. At the present time it has only been possible to measure the intensities of lines and we now consider what we can learn from such measurements.

Following Pottasch (1964) we can write the intensity of a line as

$$E = 7.75 \times 10^{-43} g f A_z \int G(T_e) N_e^2 \, dV, \tag{2}$$

where

$$G(T_e) = T_e^{-0.5} 10^{-\left(5040 \frac{E_0}{T_e}\right)} A_{zi} \tag{3}$$

g is a Gaunt factor; f is the oscillator strength of the transition being considered; A_Z is the abundance of the element relative to hydrogen; T_e is the electron temperature; and A_{zi} is the fraction of element z in ionisation state i at temperature T_e.

If an active region were isothermal it would be a trivial problem to solve Equation (2), however, in general, an active region contains material at a variety of temperatures. A single ion is observed to radiate over a range of temperatures and this range can be much less than the range of temperatures in an active region. Thus it is important to observe a number of lines which cover a wide range of temperatures rather than just one or two lines. The resonance and Lα lines of He- and H-like ions of O, Ne, Mg, Si

have generally been used as these are strong lines and the atomic physics of such simple ions is relatively well understood. Figure 6 illustrates the function $G(T_e)$ (Jordan, 1969) for several He-like resonance lines and clearly shows the importance of observing several lines from an active region.

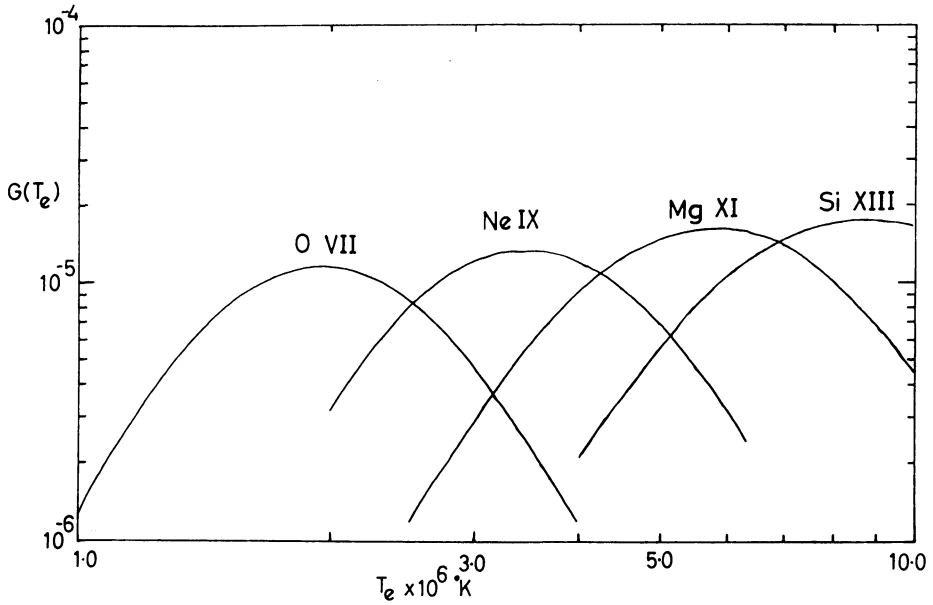

Fig. 6. Curves of $G(T_e)$ calculated using Equation (3) and the ionisation balance of Jordan (1969).

The method of analysis developed by Batstone *et al.* (1970) replaces the integral in Equation (2) by summation over several temperature intervals of width ΔT_e, thus

$$E = 7.75 \times 10^{-43} g f A_z \sum_{\Delta T_e} G(T_e) (N_e^2 V)_{T_e}. \tag{4}$$

A number of lines covering a wide range of temperatures were used and a set of over-determined simultaneous equations was solved to give an emission measure, $N_e^2 V$, variation with temperature, T_e.

Chambe (1971) has since suggested a method which assumes a differential emission measure of the form

$$\frac{\mathrm{d}}{\mathrm{d}T_e} \int N_e^2 \, \mathrm{d}V = C \times 10^{-T_e/T_0}, \tag{5}$$

where C and T_0 are constants which are determined from the analysis. This method is useful when only a few lines have been observed.

After the temperature structure of a plasma has been diagnosed by using the intensities of several lines it is possible to use the model to estimate oscillator strengths and collision strengths for ions that were not used in constructing the model.

It seems worthwhile at this point to illustrate this model fitting procedure with a spectrum I obtained with a spectrometer launched at 0529 UT on 30 November 1971 from Woomera, South Australia. The spectrometer contained three (ADP, Gypsum and KAP) crystals each with an effective area of 50 cm^2 and collimated to 3′ FWHM. The whole payload was pointed at N15 W35 (McMath Region 11621), however a small error in the pointing control system meant the centre of the active region was not viewed with maximum collimator efficiency. All three systems gave good spectra, and absolute intensities for 98 lines between 9 and 22.5 Å were measured using the reflectivities of Leigh and Evans (1972). Where the same strong line was observed on two or more crystals the intensities always agreed to better than 25%.

TABLE I

Intensities, oscillator strengths and abundances for the prime lines of O VII, O VIII, Ne IX, Ne X and Mg X

Ion	Line intensity, E 10^{-6} erg cm^{-2} s^{-1}	Oscillator strength f	Abundance $A_z \times 10^{-5}$	$\Sigma_{\Delta Te}(N_e^2 V)_{Te}$ $G(T_e) \times 10^{41}$
O VII	91.0	0.69	50	17.0
O VIII	120.0	0.42	50	36.8
Ne IX	24.4	0.73	7	30.8
Ne X	4.7	0.42	7	10.3
Mg XI	8.2	0.74	6	11.9

TABLE II

A model of an active region based on Equation (4) and Table I

Temperature interval $T_e \times 10^6$ K	Emission measure $N_e^2 V \times 10^{47}$ cm^{-3}
1.5–2.5	0.8
2.5–3.5	1.5
3.5–4.5	0.6
4.5–5.5	0.1

Table I shows the intensities of the prime lines of O VII, O VIII, Ne IX, Ne X and Mg XI together with the oscillator strength and abundances used (Pottasch, 1967). A model was constructed from this data using Equation (4) and is shown in Table II. We will refer back to this model and illustrate its usefulness later in the paper.

IV. Helium-like Ions

(a) THE 2^3S FORBIDDEN LINE

As the spectral resolution of the early observations increased it became apparent that on the long wavelength side of the helium-like resonance and intercombination lines there was a further line almost as strong as the resonance line. This was interpreted by

https://doi.org/10.1017/S0074180900071539 Published online by Cambridge University Press

Gabriel and Jordan (1969a) as due to the magnetic dipole transition $1s^2\,.\,^1S_0$–$1s2s\,.\,^3S_1$ which had previously been assumed to decay by a two-photon process. Gabriel and Jordan (1969b) investigated interchange between the 2^3S and 2^3P levels and found that as the density increased so the collision rate $2^3S \rightarrow 2^3P$ increased and competed with the spontaneous decay of the 2^3S level. In this way the intensity ratio, R, of the forbidden to the intercombination line depends on the electron density, N_e. Solving the statistical equilibrium equations for the ground state and the six $n=2$ levels gives

$$R = \frac{A(2^3S \rightarrow 1^1S)}{N_e C(2^3S \rightarrow 2^3P)(1+F) + A(2^3S \rightarrow 1^1S)} \left(\frac{1+F}{B} - 1 \right) \tag{6}$$

(neglecting photo-excitation from 2^3S to 2^3P), where

$$F = \frac{C(1^1S \rightarrow 2^3S)}{C(1^1S \rightarrow 2^3P)} \tag{7}$$

and is usually taken as 0.35.

The effective branching ratio

$$B = \frac{1}{3} \frac{A(2^3P_1 \rightarrow 1^1S)}{A(2^3P_1 \rightarrow 1^1S) + A(2^3P \rightarrow 2^3S)} + \frac{5}{9} \frac{A(2^3P_2 \rightarrow 1^1S)}{A(2^3P_2 \rightarrow 1^1S) + A(2^3P \rightarrow 2^3S)},$$

where the A's are spontaneous decay rates, and the C's are collision rates.

For low densities the collision rate $2^3S \rightarrow 2^3P$ will be small compared to the spontaneous decay rate $2^3S \rightarrow 1^1S$ and R will have a maximum value of

$$R_0 = \left(\frac{1+F}{B} - 1 \right). \tag{9}$$

It is only when the density has increased sufficiently that the value of R will deviate from the value R_0. The density at which this happens is called the critical density and using the best available data Gabriel and Jordan (1972) give values of 7.3×10^9 cm^{-3} for O VII, 1.5×10^{11} cm^{-3} for Ne IX, 1.8×10^{12} cm^{-3} for Mg XI and 1.3×10^{13} cm^{-3} for Si XIII. Apart from the value for O VII these densities are much higher than are currently believed to exist in active regions.

The observations of Acton *et al.* (1972) referred to earlier have allowed them to directly measure the ratio R for O VII and Ne IX in several active regions during their rocket flight. Chambe's exponentially decreasing emission measure model was used and a characteristic temperature for the formation of each ion in each active region was deduced. The temperature dependence of the ratio R was calculated by Blumenthal *et al.* (1972) who found a strong dependence on temperature. Gabriel and Jordan (1973) disputed their calculations on the grounds that they had treated the contribution from dielectronic recombination incorrectly so finding a strong dependence on

temperature. Figure 7 shows the calculations of Blumenthal *et al.* and Gabriel and Jordan together with the observations of Acton *et al.* for O VII and Ne IX. We conclude that there has been no observed variation of R with temperature, but under certain particular circumstances variations from the low density limit may be found.

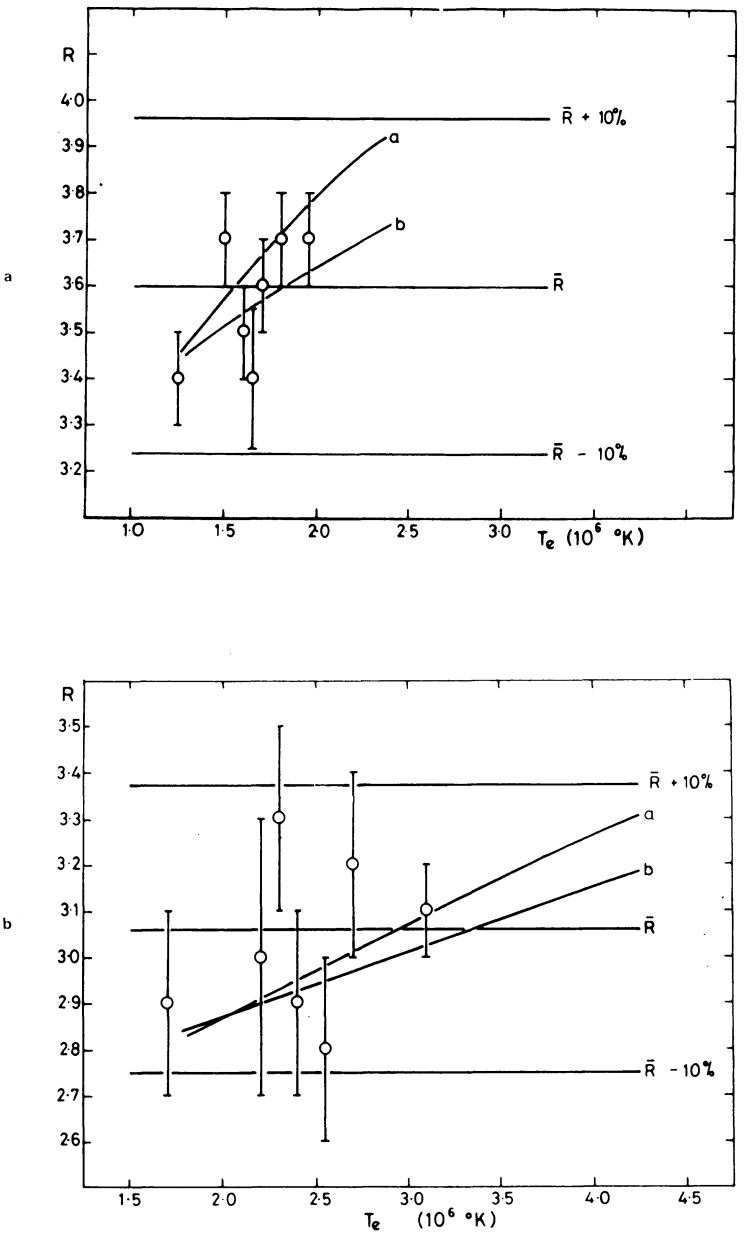

Fig. 7. The variation of R with T_e. (a) O VII. (b) Ne IX. The observations are by Acton *et al.* (1972), curve (a) is calculated by Blumenthal *et al.* (1972) and curve (b) by Gabriel and Jordan (1973).

https://doi.org/10.1017/S0074180900071539 Published online by Cambridge University Press

(b) SATELLITE LINES

Greater spectral clarity and increased instrument sensitivity also led to the discovery of satellite lines on the long wavelength side of He-like resonance lines. The satellite lines had been observed in laboratory plasmas for a number of years (e.g. Edlen and Tyren, 1939) and they were classified as being transitions of the type

$$1s^2 . n1 - 1s2p . n1 .$$

It was the observation of such lines in the solar X-ray spectrum that prompted theoretical studies of the configurations giving these lines.

We have already seen that the observations of Acton *et al.* (1972) in Figure 4 show satellite lines in He-like Ne and O. Similar data has been obtained by Walker and Rugge (1971) for silicon.

Figure 8 is a scan through the lines of Mg XI and shows many satellites clearly resolved (Parkinson, 1972). The letters refer to the transitions listed in Table III. A similar spectrum has been reported by Bonnelle *et al.* (1973) from the experiment discussed in Section 2. The lines marked R_3 are from transitions

$$1s^2 2s . {}^2S_{1/2} - (1s2p\ {}^1P)\ 2s . {}^2P_{3/2,1/2}$$

those marked R_4 are from

$$1s^2 2p . {}^2P_{1/2,3/2} - 1s2p^2 . {}^2D_{3/2,5/2}$$

R_1 and R_2 are

$1s^2 . n1 - 1s2p . n1$ with $n=4$ and 3 respectively (Summers, 1973). Figure 8 demonstrates clearly that the dominant method of formation of these weak lines is by dielectronic recombination rather than by direct excitation of inner shell electrons. This is because all of the lines from transitions of the type $1s^2 . 21 - 1s2p . 21$, for which the upper levels are auto-ionising in the LS approximation with the $1s^2 + e$ continuum,

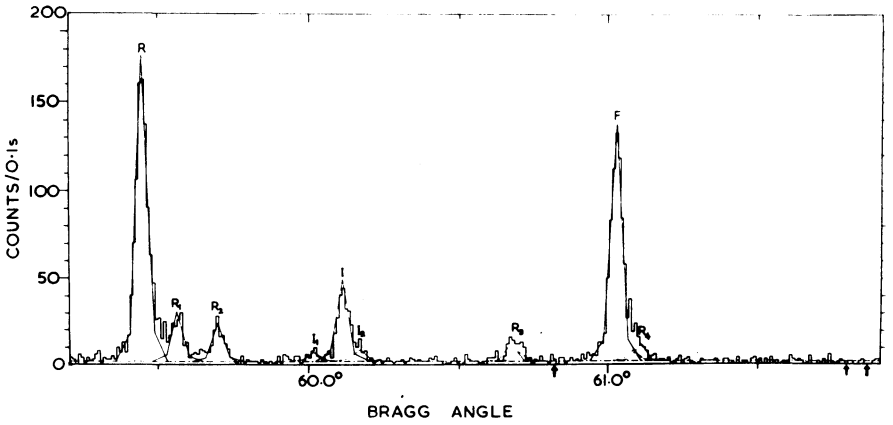

Fig. 8. The lines of Mg XI observed with a collimated ADP spectrometer (Parkinson, 1972). The letters refer to the transitions listed in Table III. The arrows indicate the positions of lines that would be produced by direct excitation of inner shell electrons.

https://doi.org/10.1017/S0074180900071539 Published online by Cambridge University Press

TABLE III

Observed and calculated wavelengths and relative intensities

	Transition		Wavelength (Å)		Relative Counts	Relative intensity	
	Lower level	Upper level	This work	Calculated		Observed	Calculated
R	$1s^2\ {}^1S_0$	$1s2p\ {}^1P_1$	9.169	9.168	885	100	100
R_1	$1s^2\ 4l$	$1s2p\ 4l$	9.180		146	16.5 ± 1.5	
R_2	$1s^2\ 3l$	$1s2p\ 3l$	9.193		115	12.9 ± 1.2	
I_1	$1s^2\ 2p\ {}^2P_{1/2}$	$1s2p^2\ {}^2S_{1/2}$	9.223	9.221	22	2.5 ± 0.7	0.5
	$1s^2\ 2p\ {}^2P_{3/2}$			9.224			1.0
I	$1s^2\ {}^1S_0$	$1s2p\ {}^3P_2$	9.232	9.227	235	26.1 ± 1.8	
		$1s2p\ {}^3P_1$		9.230			
I_2	$1s^2\ 2s\ {}^2S_{1/2}$	$(1s2p\ {}^3P)\ 2s\ {}^2P_{3/2}$	9.237	9.234	30	3.3 ± 0.7	0.7
		$(1s2p\ {}^3P)\ 2s\ {}^2P_{1/2}$		9.235			0.5
R_3	$1s^2\ 2s\ {}^2S_{1/2}$	$(1s2p\ {}^1P)\ 2s\ {}^2P_{3/2}$	9.284	9.283	56	6.2 ± 0.9	6.3
		$(1s2p\ {}^1P)\ 2s\ {}^2P_{1/2}$	9.286	9.285	29	3.2 ± 0.7	3.1
F	$1s^2\ {}^1S_0$	$1s2s\ {}^3S_1$	9.315	9.314	717	78.2 ± 3.6	
	$\ {}^2P_{1/2}$	$\ {}^2D_{3/2}$	9.319	9.320	33	3.6 ± 0.7	3.4
R_4	$1s^2\ 2p\ {}^2P_{3/2}$	$1s2p^2\ {}^2D_{3/2}$	9.323	9.323	52	5.7 ± 0.8	1.0
	$\ {}^2P_{3/2}$	$\ {}^2D_{5/2}$		9.324			5.5

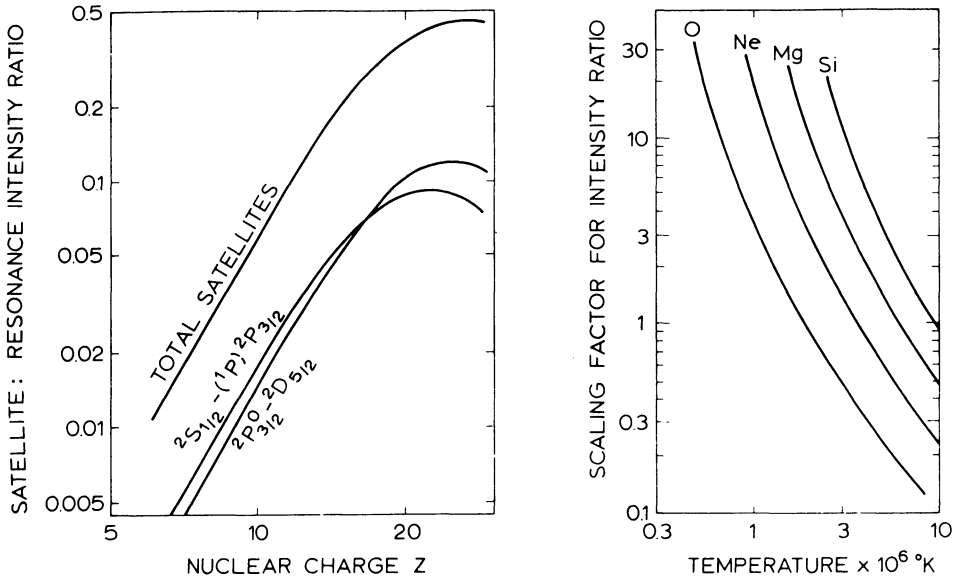

Fig. 9. Satellite line intensities (Gabriel, 1972). (a) Variations of satellite: resonance intensity ratio with nuclear charge, Z, at the characteristic temperature T_m. (b) Scaling factors for intensity ratios at other temperatures.

are observed and none of the lines from non-auto-ionising upper levels (e.g. $1s^2 2p\,.\,^2P - 1s2p^2\,.\,^2P$ at 9.302 Å) are observed.

Note that the absolute wavelength accuracy of the strong lines here is ± 0.001 Å and the resolving power of this spectrometer, using an ADP crystal is close to 5000.

The intensity of these satellite lines has been investigated in detail by Gabriel (1972). He found that the ratio of the intensity of the lines marked R_3 in Figure 8 to the intensity of the resonance line, R, is strongly temperature dependent. Figure 9 summarises these calculations and shows how the satellite line intensity varies with nuclear charge, Z, and with temperature. Thus the observations of the satellite lines is another important diagnostic tool since the variation of the satellite line intensity with temperature is different from the variation of the resonance line intensity with temperature.

TABLE IV

Relative intensities of the O, Ne and Mg lines emitted at different temperatures

Ion	Temperature interval $\times 10^6$ K			
	1.5–2.5	2.5–3.5	3.5–4.5	4.5–5.5
O VII	0.56	0.40	0.04	–
O VIII	0.17	0.63	0.19	0.01
Ne IX	0.09	0.63	0.25	0.03
Ne X	–	0.25	0.61	0.14
Mg XI	0.02	0.40	0.46	0.12

https://doi.org/10.1017/S0074180900071539 Published online by Cambridge University Press

We are now in a position to compare the accuracy of Gabriel's calculated variation of satellite resonance intensity with the observations in Figure 8 and the model in Table II. Table IV lists the fraction of each line emitted in each temperature bin so by reference to Figure 9 we can predict a satellite: resonance ratio for the whole model. This gives

Ratio satellite, R_3: resonance, R

	Observed	Predicted
Ne IX	0.017	0.039
Mg XI	0.093	0.130

The line R_3 is somewhat weaker than predicted, this may be due to slight errors in the rate coefficients used. For Mg XI we can compare the ratio of R_3:R_4 and find good agreement between the observed ratio of 9.4:9.3 and the predicted ratio of 4.6:4.5.

V. Hydrogen-Like Ions

The ratio of the intensities of the Lα and Lβ lines for a hydrogen-like ion is sensitive to temperature. Hutcheon and McWhirter (1973) have investigated this temperature variation for various density regimes. For the hydrogen-like ions observed in the solar corona and discussed in the present paper the variation is very slow, a factor two change in temperature giving only a 10% change in the Lyman ratio. Hutcheon and McWhirter point out that the laboratory theta pinch observations give measured Lyman ratios for C VI and N VII of 60–80% of their theoretically predicted values and explain the discrepancy as due to self absorption in the plasma. As recent solar observations of O VIII and Ne X give similarly reduced ratios this explanation is open to question.

Satellite lines to Lα lines have been observed in the solar spectrum of Mg XII by Walker and Rugge (1971). These lines are very weak and so may not prove to be useful for plasma diagnostic work.

VI. Neon-Like Ions

(a) Fe XVII

We have seen from Figures 1 and 2 how lines of Fe XVII dominate the solar spectrum below 25 Å. It is only recently that we have been able to account accurately for their intensities.

The strong lines correspond to transitions from the $2p^5 3s$ and $2p^5 3d$ levels to the ground state $2p^6\,.\,^1S_0$ and occur around 17 Å and 15 Å respectively. It has long been recognised (Pottasch, 1966) that each excited level cannot be accounted for by the simple coronal equilibrium conditions, where excited levels are populated solely by collisional excitation. The early theoretical studies Garstang (1966) and Froese (1967)

https://doi.org/10.1017/S0074180900071539 Published online by Cambridge University Press

did not allow for the population of certain levels by cascades from higher levels. An investigation by Beigman and Urnov (1969) showed the true complexity of the problem in that the $2p^5 3s$ levels are populated by the cascade chain.

$$2s2p^6 3d \rightarrow 2s^2 2p^5 3d \rightarrow 2s^2 2p^5 3p \rightarrow 2s^2 2p^5 3s$$

Unfortunately they were only able to treat the complete multiplets and were not able to deal with individual transitions. The problem has recently been solved by Loulergue and Nussbaumer (1973) who considered excitations to and cascades between 36 levels, and calculated the relative intensities of the 8 observed lines for transitions from $2p^5 3s$, $2p^5 3d$ and $2s2p^6 3p$ to the ground state. These relative intensities were found to be in agreement with the recent observations of Parkinson (1973) shown in Figure 10.

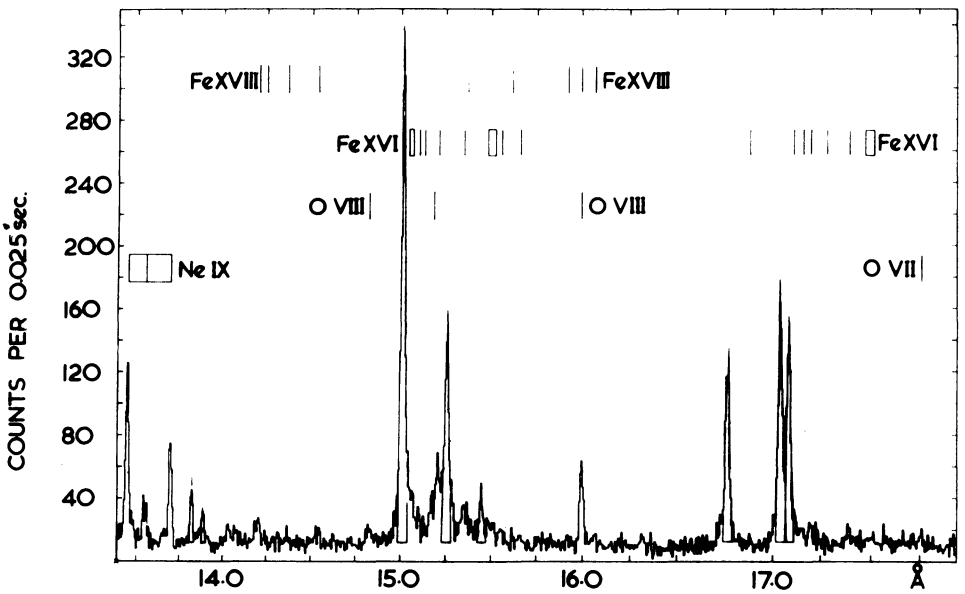

Fig. 10. Part of a collimated spectrum showing the dominance of Fe XVII between 13 and 18 Å. (Parkinson, 1973). The intensities of these lines are given in Table V.

In the light of the more recent observations it is now clear that the line ratios derived from older observations are considerably in error, mainly because the Fe XVII lines had not been clearly resolved. Figure 11 shows the $2p^5 3s$ lines around 17 Å. This section of spectrum is particularly interesting as the $^3P_1$ and $^3P_2$ lines at 17.041 and 17.086 Å are clearly resolved. The $^3P_2$ transition is particularly interesting as this is a magnetic quadrupole transition, i.e. $\Delta J = 2$, the $^3P_2$ level being the lowest level of the first excited state (Garstang, 1969).

Many of the energy levels giving higher transitions in Fe XVII are not known accurately and extrapolations along series' are difficult. The $2p^5 4d$ lines at 12 Å are well

https://doi.org/10.1017/S0074180900071539 Published online by Cambridge University Press

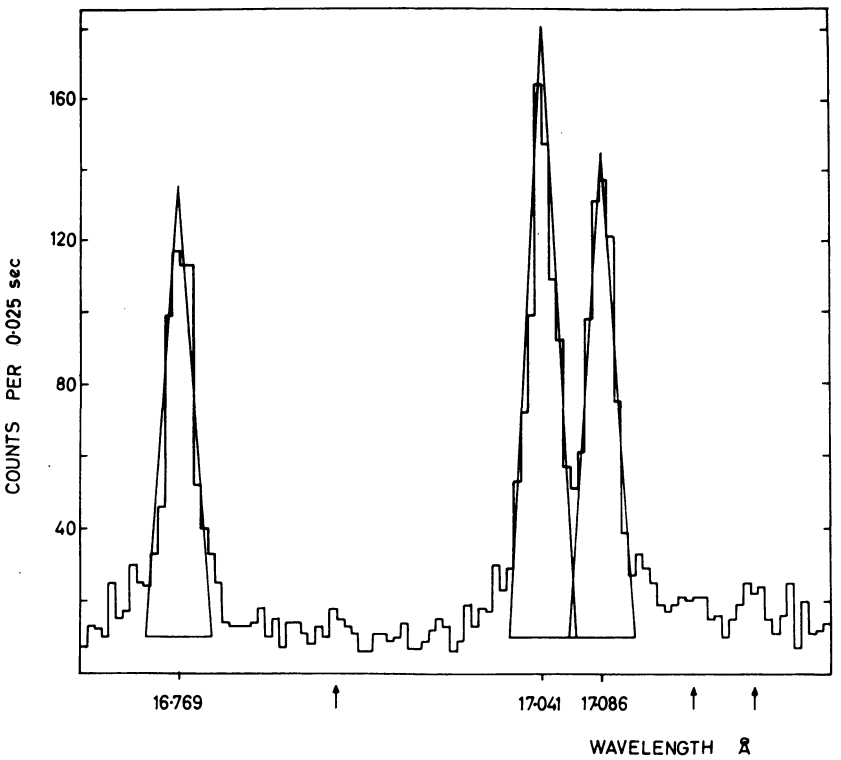

Fig. 11. Enlargement of part of Figure 10 showing the 3*s* Fe XVII lines at 17 Å. The $^3P_1$ and $^3P_2$ lines at 17.041 and 17.086 Å are clearly resolved. The arrows denote the positions of possible satellite lines.

known but the $4d\,.\,^1P_1$ resonance line at 12.121 Å is generally blended with the Ne X Lα line at 12.132 Å. Figure 12 shows these lines clearly resolved for the first time together with the $4d\,^3D_1$ line at 12.263 Å for comparison. The observed ratio of $^1P_1/^3D_1$ is 1.2 and this compares very favourably with the value of 1.1 calculated by Froese. The $5d\,^1P_1$ and $^3D_1$ lines are identified at 11.130 and 11.251 Å and the $6d\,^1P_1$ and $^3D_1$ lines at 10.660 and 10.771 Å. The ns series is more difficult, the 4*s* lines are expected to lie between 12.50 and 12.80 Å but this region of the spectrum is very crowded as can be seen in Figure 13 which shows the same section of spectrum observed simultaneously on a KAP and a Gypsum crystal.

(b) RELATIVE INTENSITIES OF Fe XVII LINES

Loulergue and Nussbaumer referred all of their intensities to the $3d\,^1P_1$ line at 15.013 Å as the population of this upper level by cascades was very small. If a reliable oscillator strength for this line can be calculated then by using the model in Table II the abundance of Fe can be calculated. To a first approximation I have used the oscillator strength of Froese of 2.22 and this gives an Fe abundance of 6.4×10^{-5} in good agreement with the value obtained by Pottasch (1967) of 6.5×10^{-5}.

https://doi.org/10.1017/S0074180900071539 Published online by Cambridge University Press

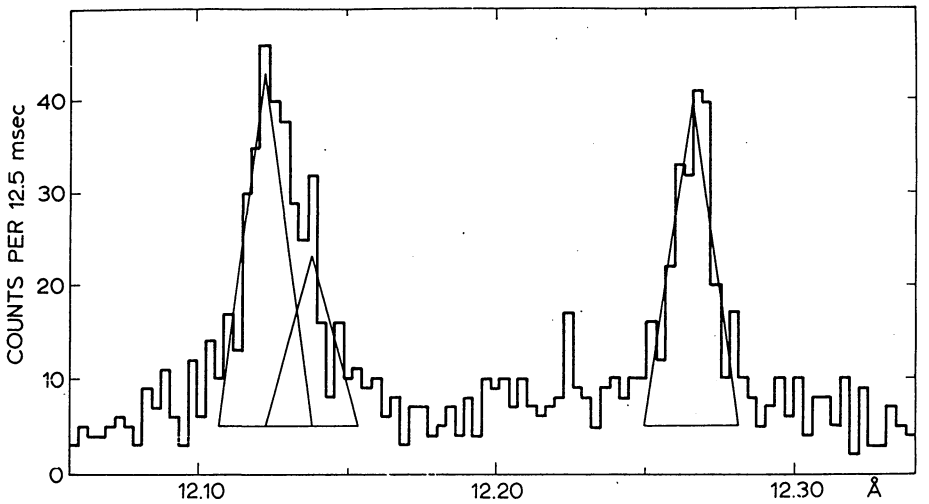

Fig. 12. A continuation of the spectrum in Figure 10 showing the 4*d* Fe XVII lines at 12 Å. The $4d\,^1P_1$ Fe XVII line at 12.121 Å and the Ne x Lα line at 12.132 Å are clearly resolved.

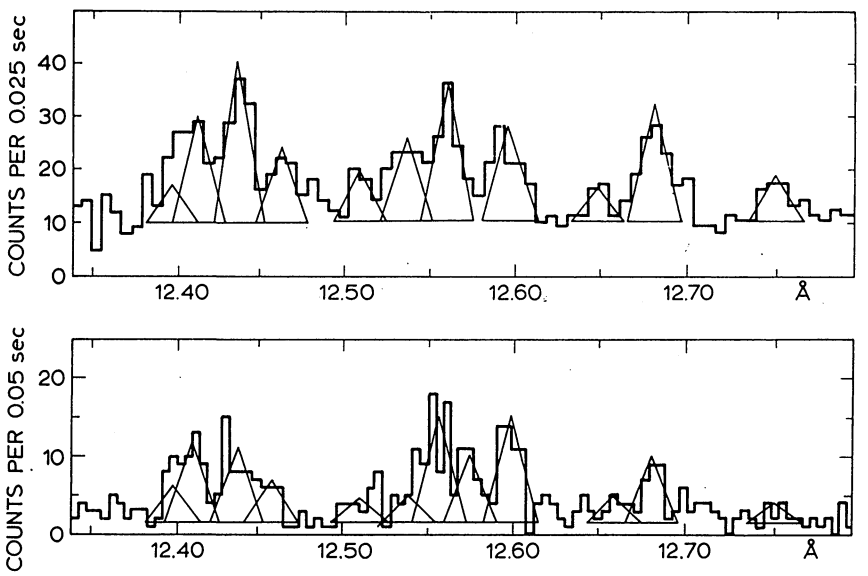

Fig. 13. The complex spectrum between 12.3 and 12.8 Å observed simultaneously with collimated KAP (upper) and Gypsum (lower) crystals. The Ni XIX 3*d* lines are at 12.436 and 12.659 Å; the Fe XVII $4d\,^3P_1$ and 4*s* lines also occur in this part of the spectrum.

In Table V I have listed all of the other Fe XVII lines that it has been possible to identify together with their intensities relative to the 15.013 Å line. Using the abundance just derived I have calculated oscillator strengths and collision strengths. These are also given in Table V.

https://doi.org/10.1017/S0074180900071539 Published online by Cambridge University Press

TABLE V

Observed intensities of Fe XVII lines relative to the intensity of 15.013 Å line

Transition		Observed			
Lower level	Upper level	Wavelength λ, Å	Intensity E, $\times 10^{-6}$ erg cm^{-2} s^{-1}	Oscillator strength f	Effective collision strength
$1s^22s^22p^6.{}^1S_0$	$1s^22s^22p^53s.{}^1P_1$	16.769	71.6	0.94	0.050
$1s^22s^22p^6.{}^1S_0$	$1s^22s^22p^53s.{}^3P_1$	17.041	103.7	1.35	0.074
$1s^22s^22p^6.{}^1S_0$	$1s^22s^22p^53s.{}^3P_2$	17.086	81.8	1.07	0.058
$1s^22s^22p^6.{}^1S_0$	$1s^22s^22p^53d.{}^1P_1$	15.013	111.3	2.22	0.107
$1s^22s^22p^6.{}^1S_0$	$1s^22s^22p^53d.{}^3D_1$	15.259	53.4	1.06	0.052
$1s^22s^22p^6.{}^1S_0$	$1s^22s^22p^53d.{}^3P_1$	15.449	12.8	0.26	0.013
$1s^22s^22p^6.{}^1S_0$	$1s^22s\ 2p^63p.{}^1P_1$	13.824	7.9	0.21	0.009
$1s^22s^22p^6.{}^1S_0$	$1s^22s\ 2p^63p.{}^3P_1$	13.889	4.4	0.12	0.005
$1s^22s^22p^6.{}^1S_0$	$1s^22s^22p^54s.{}^1P_1$	12.509	1.0	0.04	0.001
		12.599	2.8	0.10	0.004
$1s^22s^22p^6.{}^1S_0$	$1s^22s^22p^54s.{}^3P_1$	12.681	2.6	0.09	0.004
		12.751	0.9	0.03	0.001
$1s^22s^22p^6.{}^1S_0$	$1s^22s^22p^54d.{}^1P_1$	12.121	10.5	0.37	0.014
$1s^22s^22p^6.{}^1S_0$	$1s^22s^22p^54d.{}^3D_1$	12.263	8.8	0.31	0.012
$1s^22s^22p^6.{}^1S_0$	$1s^22s^22p^54d.{}^3P_1$	12.398	1.0	0.04	0.001
		12.409	2.6	0.09	0.004
$1s^22s^22p^6.{}^1S_0$	$1s^22s^22p^55d.{}^1P_1$	11.130	2.9	0.13	0.005
$1s^22s^22p^6.{}^1S_0$	$1s^22s^22p^55d.{}^3D_1$	11.251	3.2	0.14	0.005
$1s^22s^22p^6.{}^1S_0$	$1s^22s^22p^56d.{}^1P_1$	10.660	1.3	0.06	0.002
$1s^22s^22p^6.{}^1S_0$	$1s^22s^22p^56d.{}^3D_1$	10.771	2.0	0.09	0.003

(c) Ni XIX

Ni XIX is also a Ne-like ion but makes a much weaker contribution to the solar spectrum than Fe XVII due to its low abundance and the higher temperatures needed to excite the ion. The Ni XIX $3s\ {}^1P_1$, ${}^3P_1$ and ${}^3P_2$ lines are observed at 13.776, 14.037 and 14.081 Å respectively together with the $3d\ {}^1P_1$, ${}^3D_1$ lines at 12.436 and 12.659 Å. A similar procedure to that used for Fe XVII above gives an Ni abundance of 3.6×10^{-6}, after assuming an oscillator strength of 2.2 for the $3d.{}^1P_1$ transition.

References

Acton, L. W., Catura, R. C., Meyerott, A. J., Wolfson, C. J., and Culhane, J. L.: 1972, *Solar Phys.* **26**, 183.

Batstone, R. M.: 1970, Private communication.

Batstone, R. M., Evans, K., Parkinson, J. H., and Pounds, K. A.: 1970, *Solar Phys.* **13**, 389.

Beigman, I. L. and Urnov, A. M.: 1969, *Optika Spectrosk.* **27**, 380.

Blake, R. L., Chubb, T. A., Friedman, H., and Unzicker, A. E.: 1965, *Astrophys. J.* **142**, 1.

Blumenthal, G. R., Drake, G. W. F., and Tucker, W. H.: 1972, *Astrophys. J.* **172**, 205.

Bonnelle, C., Senemaud, C., Senemaud, G., Chambe, G., Guionnet, M., Henoux, J. C., and Michard, R.: 1973, *Solar Phys.* **29**, 341.

Brabban, D. H.: 1973, Thesis, University of London.

Brabban, D. H., Glencross, W. M., and Herring, J. R. H.: 1971, *New Techniques in Space Astronomy*, p. 135.

Chambe, G.: 1971, *Astron. Astrophys.* **12**, 210.
Edlen, B. and Tyren, F.: 1939, *Nature* **143**, 940.
Evans, K. and Pounds, K. A.: 1968, *Astrophys. J.* **152**, 319.
Fritz, G., Kreplin, R. W., Meekins, J. F., Unzicker, A. E., and Friedman, H.: 1967, *Astrophys. J.* **148**, L133.
Froese, C.: 1967, *Bull. Astron. Inst. Neth.* **19**, 86.
Gabriel, A. H.: 1972, *Monthly Notices Roy. Astron. Soc.* **160**, 99.
Gabriel, A. H. and Jordan, C.: 1969a, *Nature* **221**, 947.
Gabriel, A. H. and Jordan, C.: 1969b, *Monthly Notices Roy. Astron. Soc.* **145**, 241.
Gabriel, A. H. and Jordan, C.: 1972, *Case Studies in Atomic Collision Physics* **II**, North Holland, Amsterdam, p. 109.
Gabriel, A. H. and Jordan, C.: 1973, *Astrophys. J.* **186**, 327.
Garstang, R. H.: 1966, *Publ. Astron. Soc. Pacific* **78**, 399.
Garstang, R. H.: 1969, *Publ. Astron. Soc. Pacific* **81**, 488.
Hutcheon, R. J. and McWhirter, R. W. P.: 1973, *J. Phys. B.* **6**, 2668.
Jordan, C.: 1969, *Monthly Notices Roy. Astron. Soc.* **142**, 501.
Leigh, B. and Evans, K.: 1972, Private communication.
Loulergue, M. and Nussbaumer, H.: 1973, *Astron. Astrophys.* **24**, 209.
Neupert, W. M.: 1971, *Physics of the Solar Corona*, Reidel, Holland, p. 237.
Parkinson, J. H.: 1971a, *Nature Phys. Sci.* **233**, 44.
Parkinson, J. H.: 1971b, Thesis, University of Leicester.
Parkinson, J. H.: 1972, *Nature Phys. Sci.* **236**, 68.
Parkinson, J. H.: 1973, *Astron. Astrophys.* **24**, 215.
Parkinson, J. H. and Pounds, K. A.: 1971, *Solar Phys.* **17**, 146.
Pottasch, S. R.: 1964, *Space Sci. Rev.* **3**, 816.
Pottasch, S. R.: 1966, *Bull. Astron. Soc. Neth.* **18**, 443.
Pottasch, S. R.: 1967, *Bull. Astron. Soc. Neth.* **19**, 113.
Rugge, H. R. and Walker, A. B. C.: 1968, *Space Res.* **VIII**, North-Holland, Amsterdam, p. 439.
Summers, H. P.: 1973, *Astrophys. J.* **179**, L45.
Walker, A. B. C.: 1972, *Space Sci. Rev.* **13**, 672.
Walker, A. B. C.: 1975, This volume, p. 73.
Walker, A. B. C. and Rugge, H. R.: 1971, *Astrophys. J.* **164**, 181.